JOURNAL of
MATERIALS and MECHATRONICS:A

e-ISSN 2717-8811
JournalMM, 2023, 4(1), 302-317
https://doi.org/10.55546/jmm.1296633

Araştırma Makalesi / Research Article

Effect of Boron-Aluminide Coating Applied on R4 Grade Offshore Mooring Chain Steel on Pitting and Tribo-Corrosion Behaviour

Sabri ALKAN*

Bandırma Onyedi Eylül Üniversitesi, Denizcilik Meslek Yüksekokulu, Motorlu Araçlar ve Ulaştırma Teknolojileri Bölümü, Balıkesir, Türkiye,
ORCID ID: https://orcid.org/0000-0002-1052-4778, salkan@bandirma.edu.tr

Geliş/ Received: 13.05.2023; **Kabul / Accepted:** 28.05.2023

ABSTRACT: Offshore mooring systems are susceptible to wear, corrosion, and fatigue damage, making improving their tribocorrosion resistance essential. This study aims to evaluate the effects of boron-aluminizing treatment on the corrosion and tribocorrosion resistance of R4 steel in a marine environment. The boron-aluminide coating was characterized by SEM, EDS, and XRD, revealing the presence of FeAl as the dominant phase with minor amounts of FeB, Fe_2B, and Fe_2Al_5 phases. Results showed that the boron-aluminide coating improved the corrosion resistance of R4 steel, acting as a barrier between the coating and the steel substrate and maintaining its corrosion resistance even under wear conditions. The findings suggest that the boron-aluminide coating can potentially improve the corrosion and tribocorrosion resistance of R4 steel in marine environments, making it a cost-effective alternative to passive materials for the thermochemical coating of low-alloy steels.

Keywords: HSLA steel, boro-aluminizing, corrosion, tribocorrosion, seawater

*Sorumlu yazar / Corresponding author: salkan@bandirma.edu.tr

Bu makaleye atıf yapmak için /To cite this article

Alkan, S. (2023). Effect of Boron-Aluminide Coating Applied on R4 Grade Offshore Mooring Chain Steel on Pitting and Tribo-Corrosion Behaviour. Journal of Materials and Mechatronics: A (JournalMM), 4(1), 302-317.

1. INTRODUCTION

The structural stability of floating offshore structures can be compromised by various factors, which can have catastrophic consequences. One of the leading causes of malfunctions in these structures is the damage to the mooring systems due to wear, corrosion and fatigue (Angulo et al., 2019). The links and accessories of mooring chains experience corrosion and wear as they move against each other in the dynamic marine environment, including factors like tides, waves, and currents (Alkan, 2017). Synergistic interaction between wear and corrosion speeds up each other, and material loss occurs more than in wear-alone or corrosion-alone situations (Ma et al., 2013; López-Ortega et al., 2018; Jiajia et al., 2019; Zhang and Hoogeland, 2019; Du et al., 2020). This phenomenon is known as tribocorrosion. Understanding the tribocorrosion behaviour of offshore mooring components and enhancing their tribocorrosion resistance is crucial due to replacement challenges and maintenance costs (Moghaddam et al., 2020).

Offshore mooring chains are manufactured using high-strength, low-alloy (HSLA) steel in six grades selected based on their strength properties (IACS, 2013). The alloy content of conventional carbon steels is low, and their elemental content is insufficient to form a passive protective oxide layer on their surface. For this reason, to slightly improve the corrosion resistance of typical low-alloy carbon steel, it is therefore recommended by the standards that HSLA offshore mooring steels have at least 20% molybdenum (IACS, 2013). However, the oxide layer on the surfaces of low-alloy carbon steels is not pretty protective as passive alloys, such as stainless steels, and it may decompose by mechanical effects in aggressive electrolytes. On the other hand, the ferric oxyhydroxide layer, known as rust, that develops on the carbon steel accumulates, especially in the non-abraded areas in tribocorrosion, due to the continuously developing corrosion. This rust layer causes a decrease in the corrosion rate, behaving as a coating after a certain level. This situation also causes a galvanic cell due to the potential difference between worn and unworn parts, creating micro or macro pits on the corroded surfaces. Macro or micro pits may cause a decrease in the cross-sectional areas and increases global and local tensions in the structure.

The ability of passive materials to regenerate the oxide film (repassivation), which is broken due to mechanical effects under tribocorrosion conditions, puts them in the class of corrosion and tribocorrosion-resistant materials. However, passive alloys like stainless steel and titanium are costly material groups for tribocorrosive environments compared to low-alloy carbon steels, and using these costly materials is not feasible for sizeable offshore mooring systems. To overcome this issue, thermochemical surface modifications are promising alternatives to increase the tribocorrosion resistance of HSLA carbon steels instead of costly passive materials for the marine environment (Shen et al., 2016; Günen et al., 2018; Shen et al., 2018; López-Ortega et al., 2018; López-Ortega et al., 2018; López-Ortega et al., 2019; Pandim et al., 2020). One of the most promising ways is the thermochemical coating of low alloy steels with inert boride layers after aluminizing heat treatment (Günen et al., 2022). In addition to being resistant to many corrosive liquids, boroaluminizing can also increase the tribocorrosion resistance of HSLA mooring chain steels cost-effectively. This study aims to understand the pitting and tribocorrosion behaviour of HSLA steel and improve the tribocorrosion resistance in seawater by boroaluminizing.

2. MATERIALS AND METHODS

2.1 Sample preparation and coating process

The R4 grade HSLA mooring chain steel was chosen as the base material as it is widely employed in practical applications. Furthermore, HSLA steels can be used for the pack boroaluminizing procedure. The R4 grade mooring chain steel was accurately sectioned into 23 x 10 mm pieces with a thickness of 10 mm using a precise cutting tool to prepare it for coating. The pack cementation method was used to form a boron-aluminide layer on the substrate. After being appropriately ground with 320-400-600-800-1000-1200 SiC sheets, the samples' surfaces underwent a 15-minute ultrasonic cleaning procedure in an alcohol bath.

The boroaluminizing technique uses 45% B_4C, 5% $NaBF_4$ for boronizing and 22.5% aluminium, 22.5% Al_2O_3 and %5 NH_4Cl for aluminizing. Based on boronizing powders and aluminizing powders used in previous studies, the powders were prepared in a 1/1 ratio (Günen et al., 2022). The specimens were placed inside stainless steel containers known as crucibles. Then, a 10 mm thick coating of boro-aluminizing powder was spread around each piece on all sides to generate a layer of boron-aluminide. After that, the crucibles containing the samples were inserted into a furnace heated to the aluminizing temperature of 900 ℃. The crucibles were firmly attached with fasteners and left inside the furnace for two hours. Subsequently, the furnace was turned off, and the crucible was taken out and left to cool down to room temperature. Once the samples were cooled, any remaining dust was removed from their surfaces. A diagram of the boroaluminizing process is shown in Fig. 1.

To prepare the samples, they were first embedded in bakelite and then ground using SiC ground paper ranging in size from 320G to 2000G. The ground samples were then polished with Al_2O_3 solutions of 3 µm and 1 µm until a reflective surface was achieved. Next, they were submerged in a 5% Nital solution for 6 seconds, which allowed the intricate features of the microstructure to become visible.

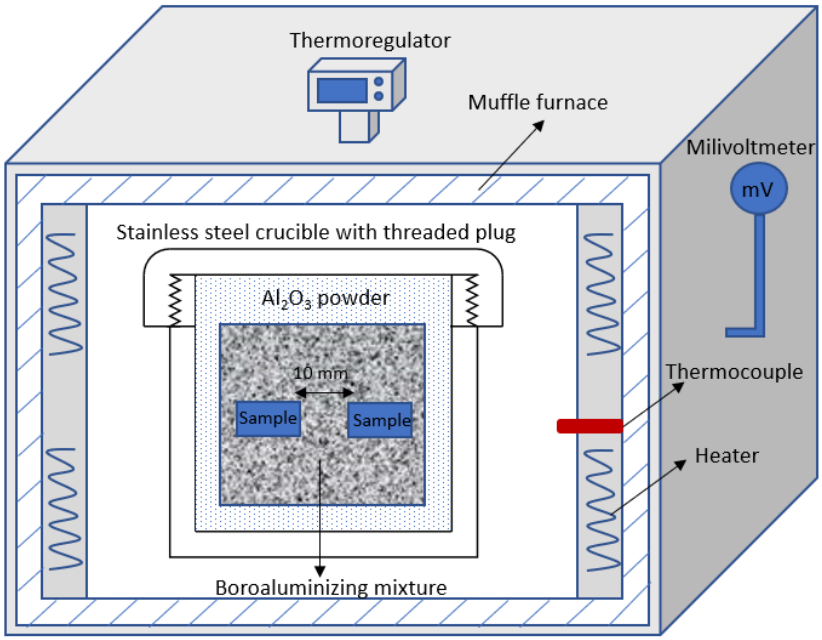

Figure 1. Schematic illustration of the boro-aluminizing setup and process

The microstructural properties and distribution of elements in the coating layer were investigated using SEM (MAIA3 XMU-TESCAN) and EDS (X-Max-OXFORD) analysis. EDS

analysis was utilized to examine how the alloying elements were distributed in the coating layer. The coating thickness was determined by measuring an average of five samples using the Fiji ImageJ measurement tool based on SEM images. To investigate the XRD patterns, Cu K radiation with a wavelength of 0.154 nm, a scan step size of 0.0525211, and 2 angles ranging from 10 to 90° were used with the Rigaku Smart LabTM.

2.2 In-situ corrosion and tribocorrosion test procedure

A reciprocating tribometer (TURKYUS) combined with a potentiostat was used to assess the tribocorrosion behaviour of HSLA steel samples with and without boron-aluminide coating in marine environments. As illustrated in Fig. 2, the experimental setup was designed to simultaneously measure wear and corrosion data during the tests (Alkan, 2022a). A 3.5% sodium chloride solution was prepared to simulate seawater for the corrosion and tribocorrosion investigations. A Delrin (a polymer material) cell containing 150 ml of the electrolyte was used for each test to avoid any unwanted electrochemical effects.

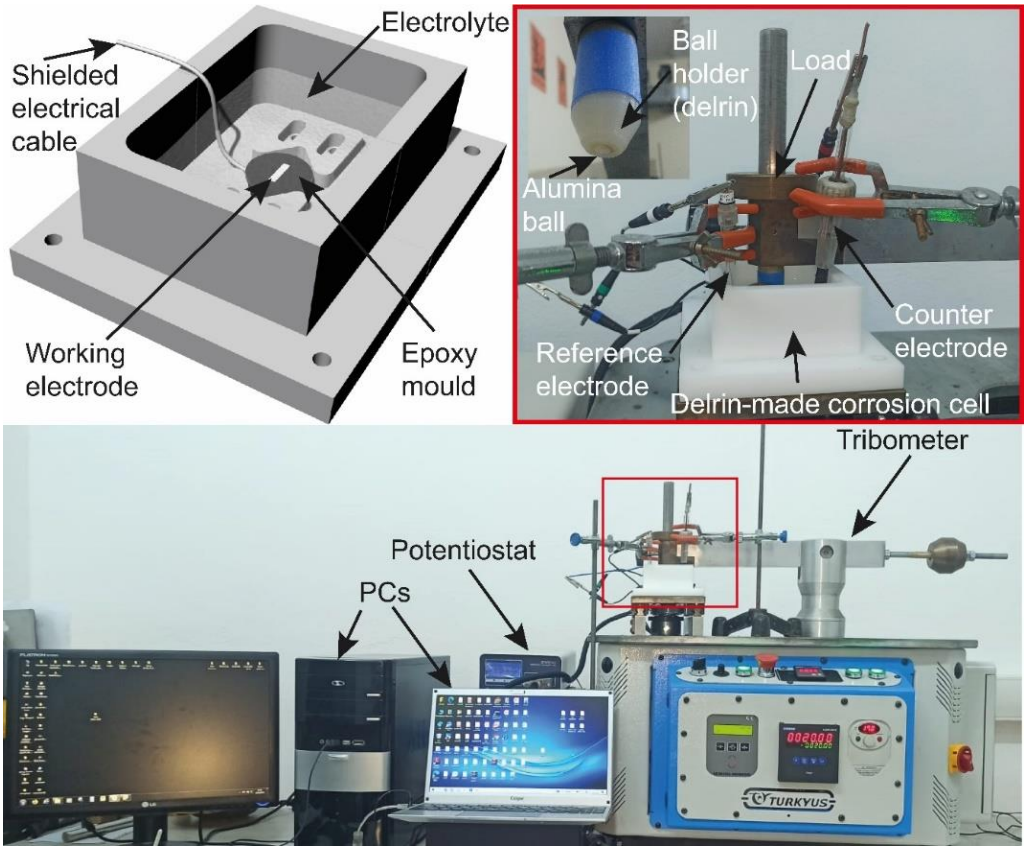

Figure 2. Setup for triboelectrochemical tests (Alkan, 2022a)

In order to conduct the sliding tests, an alumina ball (6.35 mm diameter and 14 GPa hardness) was employed as the abrasive counter body. The tests were carried out at a speed of 0.02 m/s and a sliding stroke of 6 mm, which resulted in a total wear path of 36 m under a normal load of 5 N. The samples were made sure to have a 2.3 cm^2 contact surface by coating with epoxy and then placed in a corrosion cell composed of Delrin for one hour to measure OCP. In the corrosion and tribocorrosion assessments, the coated or uncoated R4 steel samples were used as the working electrode, while platinum acted as the reference electrode and Ag/AgCl as the counter electrode. A conventional three-electrode system was used for the electrochemical tests, and the Zive SP1 analyzer test equipment

was utilized to examine the findings. The ASTM G5-14 standard was used to evaluate the electrochemical values of OCP, corrosion potential, and current density.

In this study, the impact of sliding wear on the corrosion rates of simulated seawater was investigated. Potentiodynamic polarization tests were performed under 5 N loads with scan rates of 0.166 mV/s to evaluate the corrosion resistance. The potentials ranged from 0.5 V to -1 V relative to each sample's OCP (vs Ag/AgCl). Before corrosion and tribocorrosion testing, all specimens were immersed and stabilized in the electrolyte for 3600 seconds. Each test was repeated thrice to ensure accuracy, and the average was calculated. The experiments were conducted at a temperature of 23±2 °C to maintain the consistency in the results.

2.3 Assessment of surface morphology

Following the tribocorrosion tests, the wear track dimensions were measured using a 3D laser scanning microscope from Filmetrics to determine the wear morphology. An SEM (Scanning Electron Microscope) device attached with EDS capability was also utilized to study the surface morphology of the tested samples after each test.

3. RESULTS AND DISCUSSION

3.1 Coating Characterization

Figure 3 shows the boron-aluminide layer's morphology, SEM cross-section, and EDS analysis. The boro-aluminizing process produced three visible zones, determined through EDS line analysis. Within the coating layer's 0-10 μm range, the first zone contains a distribution of approximately 70% B, 15% Fe, and 15% Al atoms at the atomic level throughout the layer. The second zone, a FeAl layer, contains equal amount of Al and Fe about (%45-50) and is located in the 10-50 micrometres range. It is clearly observed that the aluminium ratio in this region decreases as it moves away from the surface. The third region is the matrix structure unaffected by the boro-aluminizing process. It is thought that the boron content detected within this region is possibly due to the difficulty of distinguishing boron from carbon in the substrate material using EDS. Ouladsaad et al. (2019) reported that XC38 steel obtained a 44 μm thick boro-aluminide coating layer after boro-aluminizing at 900 °C for 4 hours. Thus, the coating layer produced in the research aligns with the findings in previous literature.

The EDS analysis demonstrated that the coatings had a significant amount of Al post-boron-aluminizing but lower concentrations of Fe and B within the coating layer. These EDS results supported the XRD analysis, which identified FeAl as the dominant phase in the structure with minor amounts of FeB, Fe_2B, and Fe_5Al_8 phases present. Spot EDS analyses of Fe-Al-B, Fe-Al, and the substrate material indicated that the surface layer was mainly composed of B with low levels of Fe and Al. In contrast, the second layer was composed of Fe-Al, indicating that the temperature required for aluminizing was lower than that for boronizing, leading to the formation of a Fe-Al layer on the surface followed by the beginning of boron diffusion and a decrease in Al diffusion. The substrate material contained Cr, Mn, Mo, and Fe, which were part of the grade R4 steel chemical composition and were detected through EDS analysis.

Fig. 4 illustrates the X-ray diffraction (XRD) pattern of both R4 steel and the boron-aluminide coating. As seen in Fig. 4, it was determined that R4 steel consists of ferrite and iron peaks. After boron-aluminizing, it was found that the dominant phase in the samples is FeAl, and minor amounts of FeB, Fe_2B, and Fe_2Al_5 phases are also present in the structure, as reported previously (Öksüzoğlu and Döleker, 2021). The coating structure also included $FeAl_2$, Fe_2Al_5, FeAl, and Al_5FeNi phases.

FeAl and Fe_2Al_5 phases on the surface are noteworthy since they can maintain their stability even at high temperatures, suggesting that the coating may have potential applications in high-temperature environments (Yener et al., 2019; Erdogan et al., 2021).

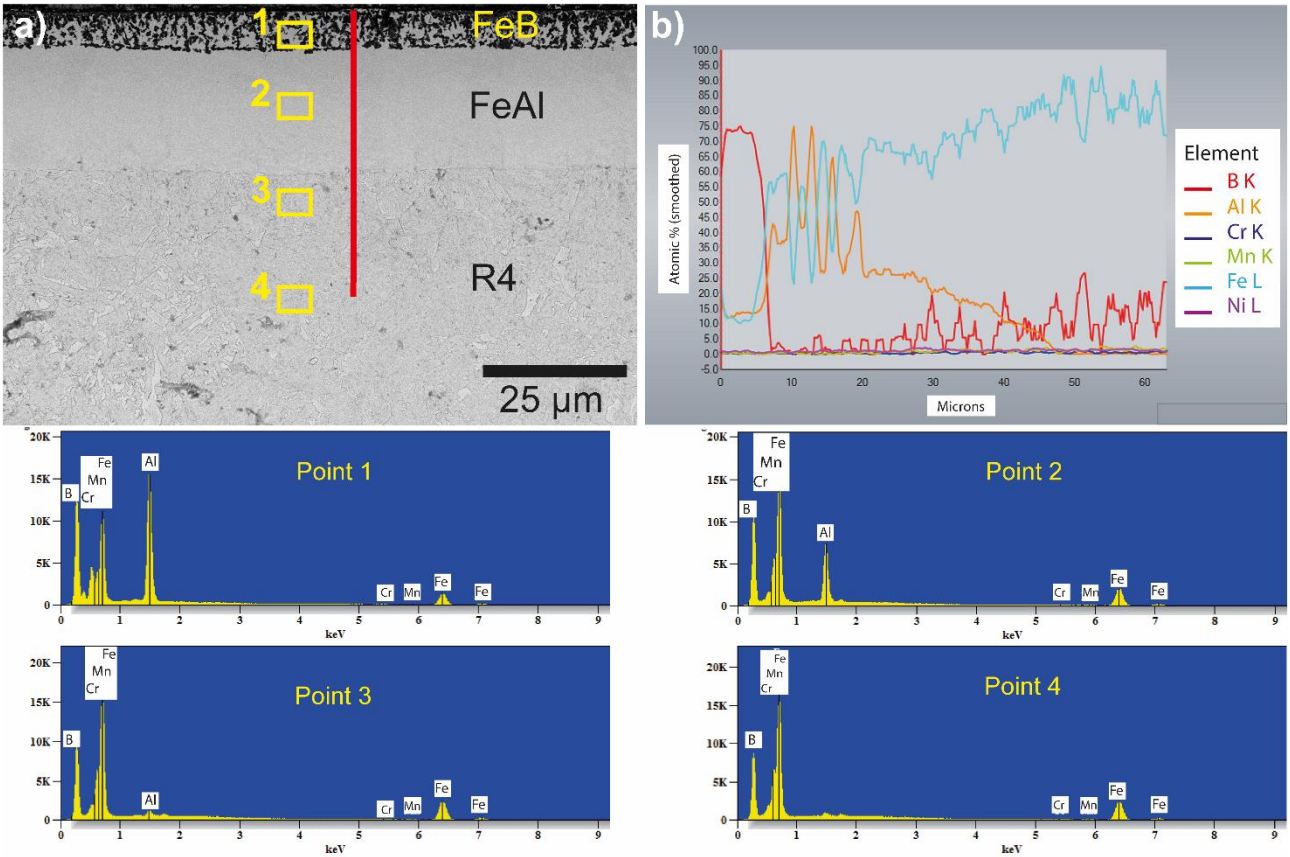

Figure 3. The microstructure and elemental composition of the boro-aluminized R4 sample

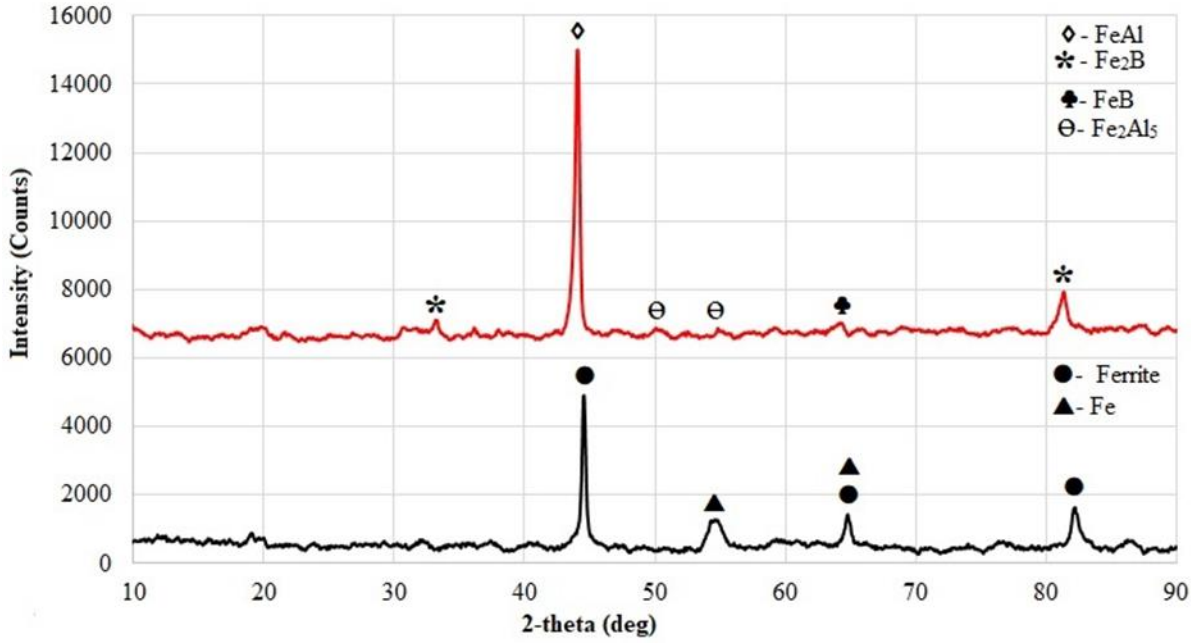

Figure 4. X-ray diffraction (XRD) analysis for R4 steel and boron-aluminide coating

3.2 Potentiodynamic polarization

The electrochemical behaviour of R4 steel and boro-aluminized R4 in 3.5% NaCl solution was investigated using Tafel plots, as shown in Fig. 5. The polarization curves obtained from the tests were used to analyze the kinetics of corrosion over a range of potentials from 0.5 V to -1 V. Table 1 summarizes the electrochemical data obtained from the polarization curves. The findings suggested that, although the corrosion potential values of the boron-aluminide coating were similar to those of the substrate, the corrosion current density was roughly double. However, the boron-aluminide coating enhanced the corrosion resistance of R4 steel, leading to lower corrosion currents, better corrosion resistance, and lower corrosion rates than untreated R4. The boron-aluminide ceramic structure and higher chemical stability in the NaCl electrolyte acted as a barrier between the coating and the steel substrate, contributing to enhanced corrosion resistance (López-Ortega et al., 2018). These results suggest that the boron-aluminide coating can improve the corrosion resistance of R4 steel in marine environments characterized by simultaneous wear and corrosion.

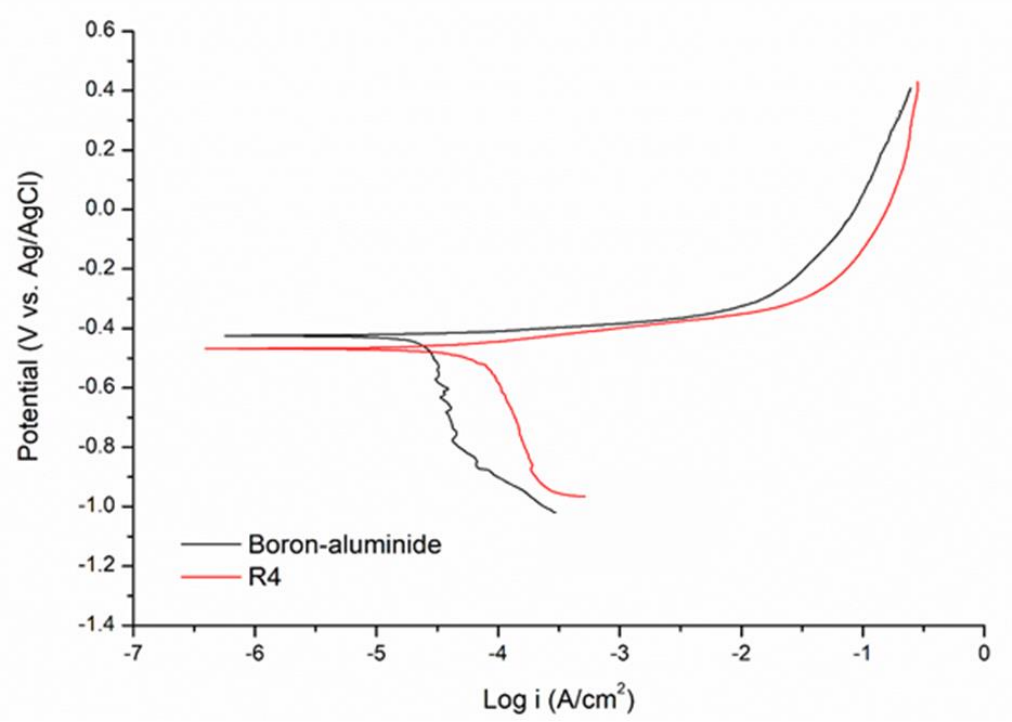

Figure 5. The Potentiodynamic scans of R4 and boron-aluminide coating under corrosion conditions

Table 1. The electrochemical data obtained from polarization curves in a 3.5% NaCl solution

	R4	**Boro-aluminized R4**
E_{corr} (mV)	-479	-424
I_{corr} (A/cm^2)	2.12E-5	1.35E-5
Corr. Rate (mmpy)	0.4730	0.2913

3.3 Assessment of OCP during corrosion and tribocorrosion

Fig. 6 (a) displays the OCPs of R4 steel and boron-aluminide coated samples immersed in a 3.5% NaCl solution for 3600 seconds. R4 steel experienced a decrease in electrochemical potential due to the continuous action of the corrosion process during the soaking time. In contrast, the boron-aluminide coating exhibited a more stable potential response between -0.50 V and -0.51 V in the first hour of immersion, thanks to forming an oxide layer with a barrier effect on the surface. After the

first hour, the potential of the boron-aluminide coating reached around -0.51 V in a simulated marine environment, indicating excellent seawater protection.

Fig. 6 (b) illustrates the changes in OCP before, during and after sliding. As a result of the sliding motion, the electrochemical potential of R4 steel shifted towards more positive values due to the disparities between the worn and unworn surfaces. This resulted in two regions behaving like batteries, with the wear track exhibiting cathodic behaviour. The ongoing mechanical activity of the counter body controlled the corrosion kinetics in the track, leading to a decrease in the corrosion rate in the wear track region of the HSLA R4 steel. Following the sliding duration, the surface of the wear track interacted with the electrolyte, forming a fresh rust layer that enabled the material to revert to nearly its initial potential values before sliding.

During the initial 900 seconds, as shown in Fig. 6(b), the potential of the boron-aluminide coating decreased to more negative values. The onset of sliding resulted in a potential difference between the two regions, as the alumina ball continuously acted on the wear track, leading to a potential shift. The OCP of the boron-aluminide layer increased due to removing the protective layer from the wear track and the electrolyte leakage onto the steel substrate. In passive surfaces, the change in the OCP under tribocorrosion usually occurs as a potential drop, although cracks or pits formed on the coating surface can cause the electrolyte to reach the substrate metal. Towards the end of the sliding period, the potential of the boron-aluminide layer dropped around 2700 s, following the re-passivation which was facilitated by the boron-aluminide surface. Furthermore, due to the aluminium's ability to form passive layers, the boron-aluminide coating could re-passivate more effectively than R4 steel (Alkan, 2022a).

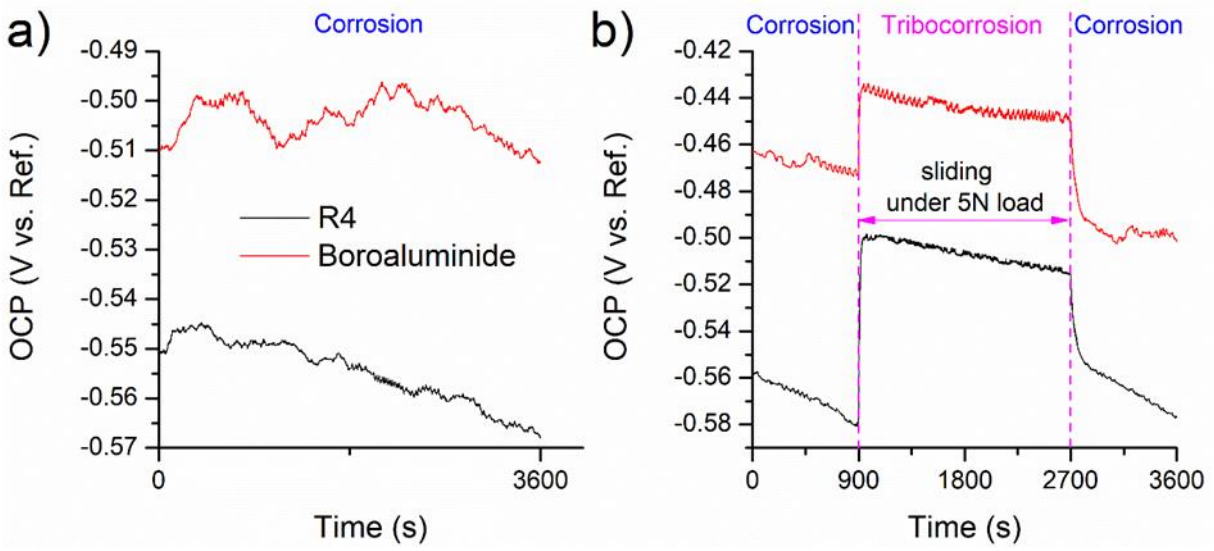

Figure 6. The electrochemical potential a) after being immersed in the solution for one hour and b) during the corrosion and sliding tribocorrosion

3.4 Examination of surface morphology

Fig. 7 displays the wear track generated on untreated R4 steel under open circuit potential (OCP) conditions after conducting tribocorrosion tests. The optical images revealed abrasive effects and micro-grooving wear marks resulting from the separation of hard oxide abrasion debris from the surface during wear, which stuck into the surface and dragged away with the counter ball. This

mechanism is well-documented in previous studies on materials with low surface hardness (Marques et al., 2011; Günen, 2016; Erdogan, 2019).

An SEM image of the wear track in Fig. 8 supported the presence of abrasive effects and material detaching under OCP conditions with corrosion processes. In Fig. 8, the corrosion products and wear debris were determined in the non-abraded region. These results could be attributed anodic behaviour of unworn surfaces and the cathodic behaviour of worn surfaces (Alkan and Gök, 2021). According to Fig. 8, pits in the unworn surface of R4 steel also support the idea of the high dissolution of material from the unworn surface. However, material detachments from the wear track, which would cause the formation of third bodies in the wear region, were determined. Another remarkable result obtained from Fig. 8 is the determination of clustered and developing micro pits in the wear track of R4 steel.

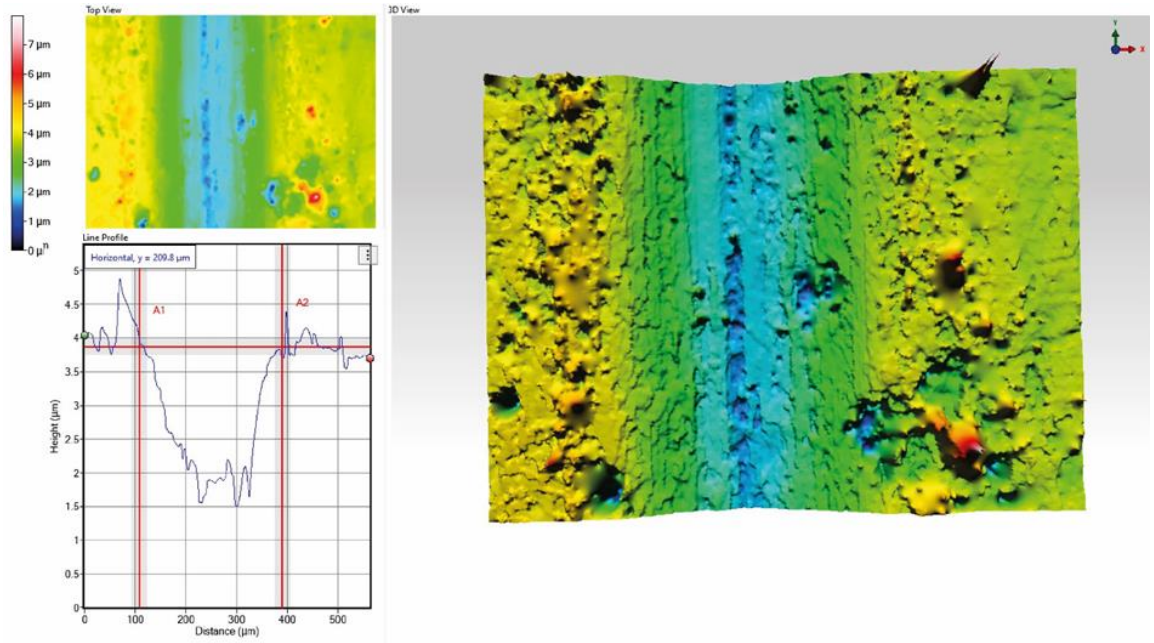

Figure 7. Optical microscopy captured after R4 steel tribocorrosion tests under OCP

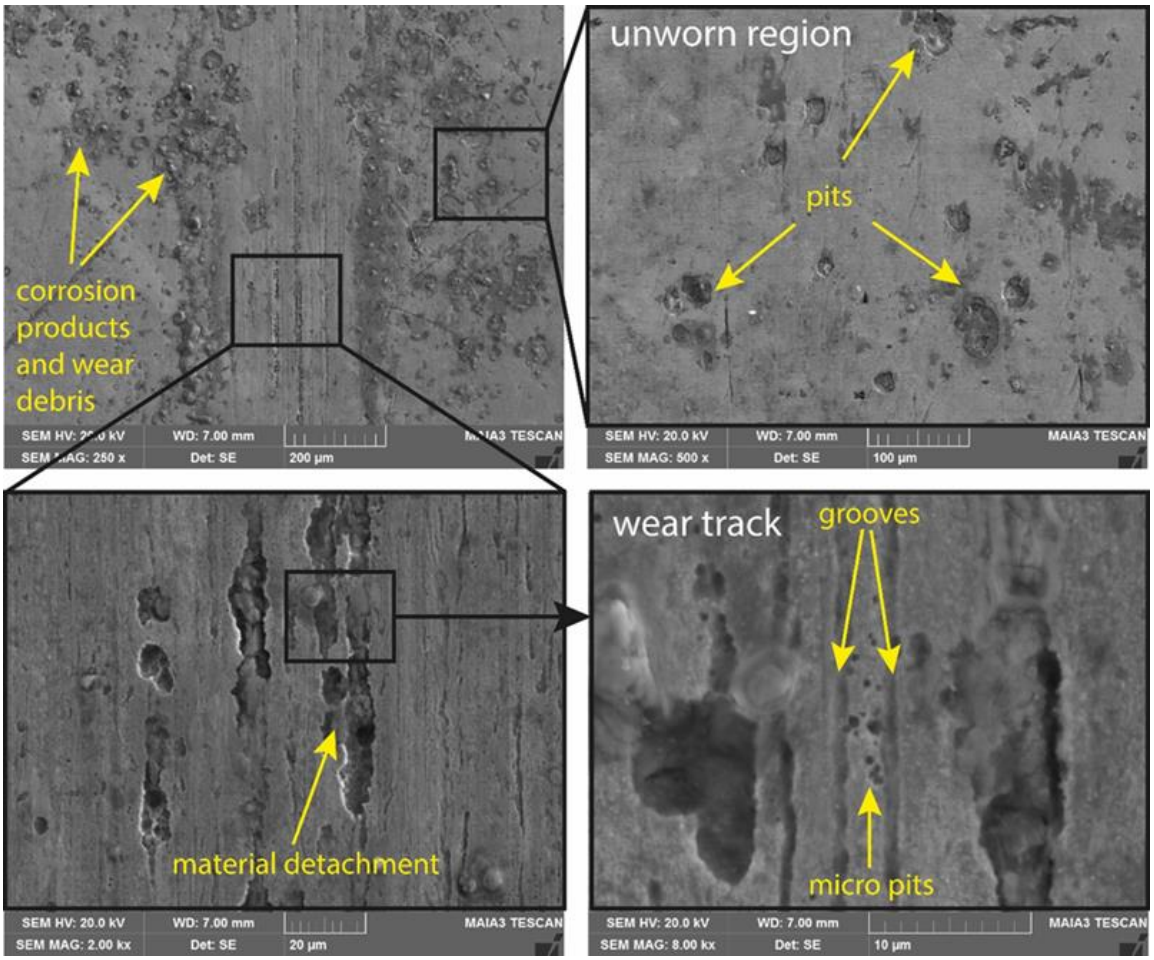

Figure 8. SEM photos of R4 steel following tribocorrosion testing under OCP

Fig. 9 shows the wear track generated on the boro-aluminized R4 under OCP in simulated seawater. Pits were visible inside and on the edge of the track, indicating pitting corrosion. The wear track surface morphology was smooth than the R4 steel track under OCP conditions. In addition, the wear track transverse section was consistent with the alumina ball. Although boron aluminide coating does not show an utterly passive behaviour in seawater like stainless steel, the formation of pits outside the trace instead of inside the track may be evidence that the coating layer exhibits a passive-like behaviour (López-Ortega et al., 2018; Alkan, 2022a). In this case, the worn region under the effect of sliding may have exhibited anodic behaviour, while the unworn regions may have performed cathodic behaviour (López-Ortega et al., 2018; Alkan and Gök, 2022).

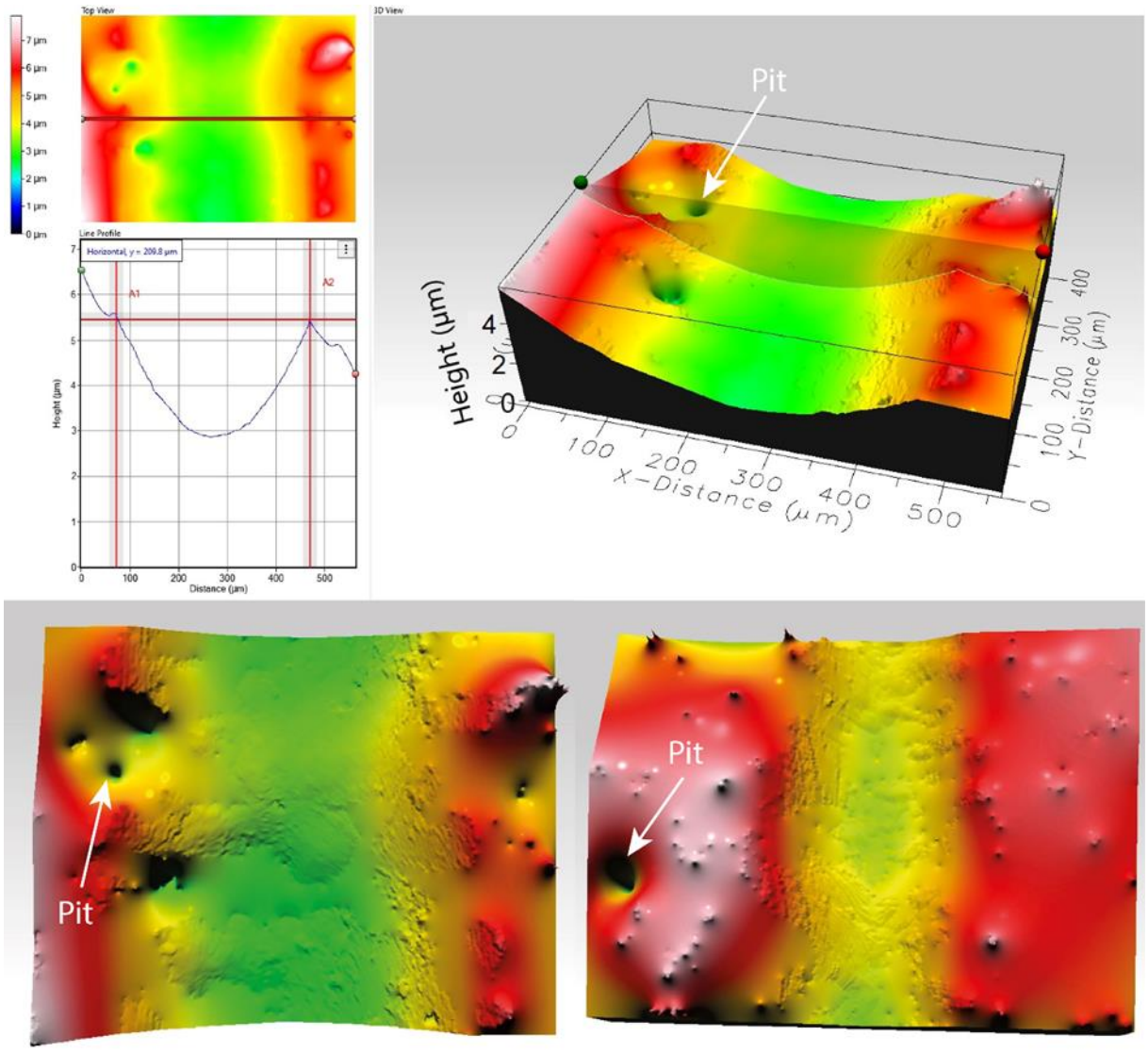

Figure 9. Optical microscope images of boro-aluminized R4 steel after open circuit potential tribocorrosion test

SEM images of wear tracks created on the surface of boro-aluminized R4 steel specimens after the tribocorrosion test are shown in Fig. 10. A few pits were observed in the unworn region, and their counts were clearly less than untreated R4 steel (Fig. 8). This result can be attributed to the formation of galvanic coupling between the worn and unworn surface of the boron aluminide layer and related to the cathodic behaviour of unworn regions during tribocorrosion. Fig. 10 displays cracks on the wear track with the corrosion process. This mechanism is explained in Fig. 11 to identify the tribocorrosion behaviour of the boron aluminide layer. According to Fig. 11, the boron aluminide coating has a rough surface morphology, and this rough morphology caused it to disable the contact counter body to the whole surface. Fig. 11 (a) explains the mechanism, and SEM images in Fig. 11 (b) support the proposed idea that the alumina counter body creates some plateaus. This mechanism produced wear particles and cracks in the wear track by shear force. However, the formation of the brittle Fe_2Al_5 phase, which was formed as a minor component along with the dominant ductile FeAl phase as determined in XRD analysis, is believed to have caused the fractures in the boron-aluminide layer (Li et al., 2021). The brittle Fe_2Al_5 intermetallic compound, which does not provide sufficient resistance against force, falls off the surface, damaging the mechanical properties of the steel under tribocorrosion conditions (Hu et al., 2006).

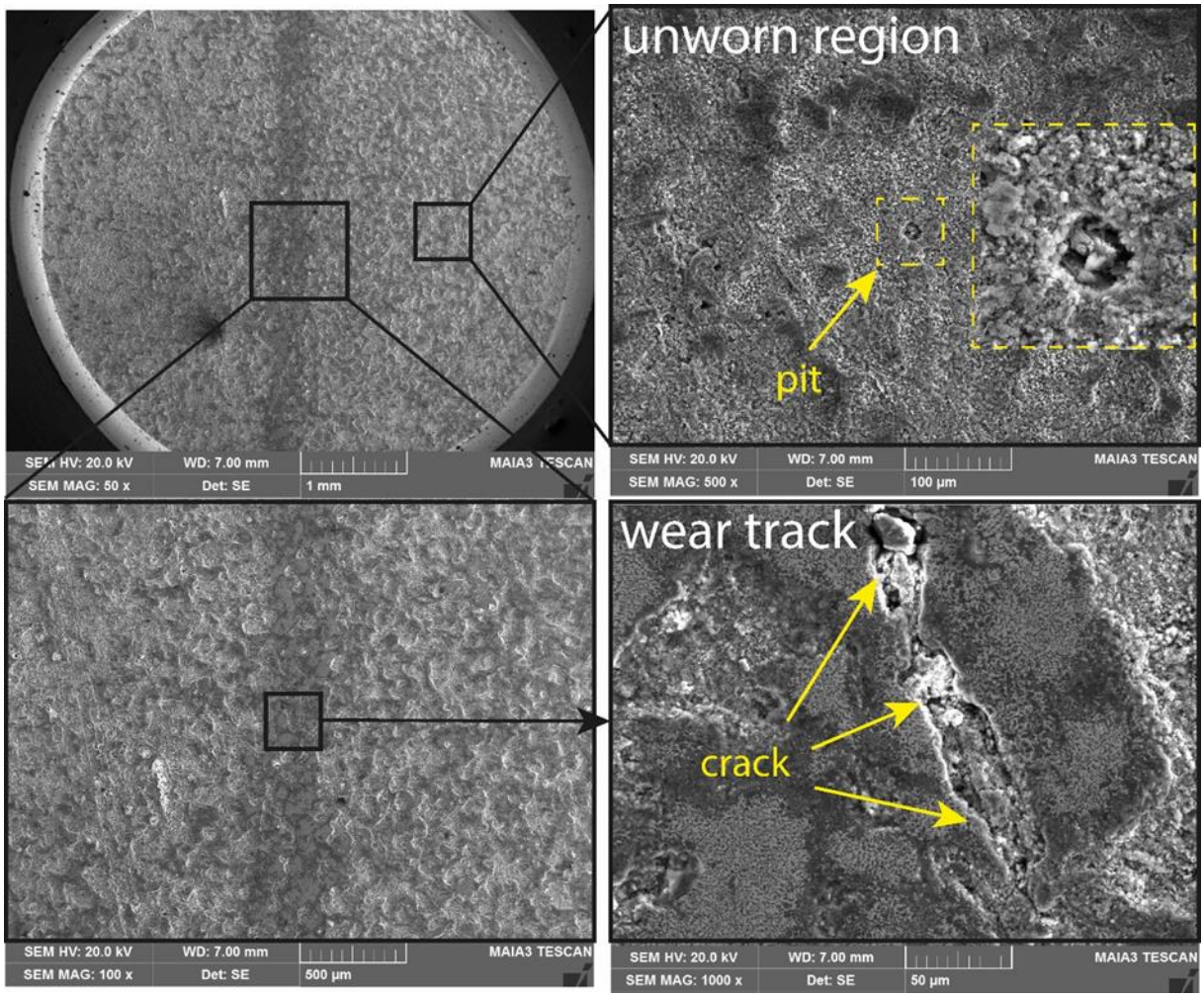

Figure 10. SEM images of boro-aluminized R4 steel following a tribocorrosion test conducted under OCP

An EDS analysis was conducted further to investigate the pitting corrosion behaviour and crack formation of boron aluminide coating, and Fig. 12 was created for this purpose. The pits and cracks contained oxides with Cl and Na ions, supporting the idea of marine corrosion. The leakage of Cl ions through pits and cracks would cause the anodic dissolution of the coating layer, a well-known phenomenon in marine tribocorrosion (Pardo et al., 2008; Zhang et al., 2015; Alkan, 2022b, 2022a).

Despite all wear and corrosion effects, when the wear track sections are compared (Fig. 7 and Fig. 9), it is seen that the boro-aluminized R4 steel has a very close wear depth (approximately 2.5 microns) and track width (approximately 300 microns) with the untreated sample. However, it should be noted that the corrosion-induced material loss of the boro-aluminide layer occurred mainly from the wear track, while the untreated sample was from the non-abraded region due to galvanic interactions. In this case, the total material loss of untreated R4 steel would be more than boro-aluminized R4. This result suggests that the boro-aluminide coating improved the tribocorrosion resistance of grade R4 offshore mooring steel.

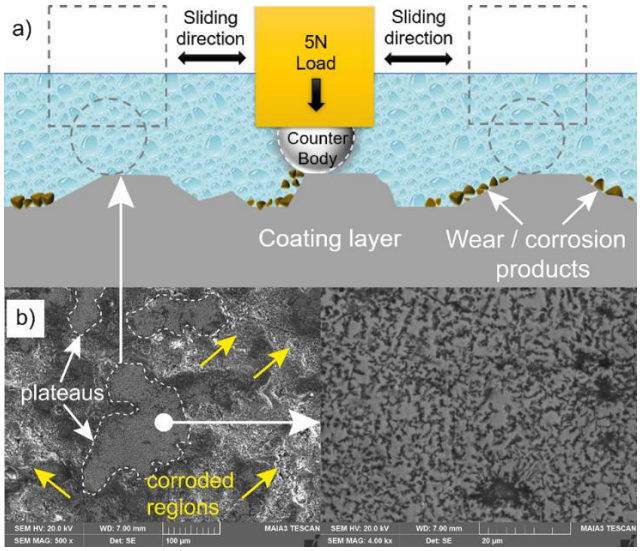

Figure 11. Tribocorrosion mechanism in the wear track: SEM images of boro-aluminized R4 steel following a tribocorrosion test conducted under OCP

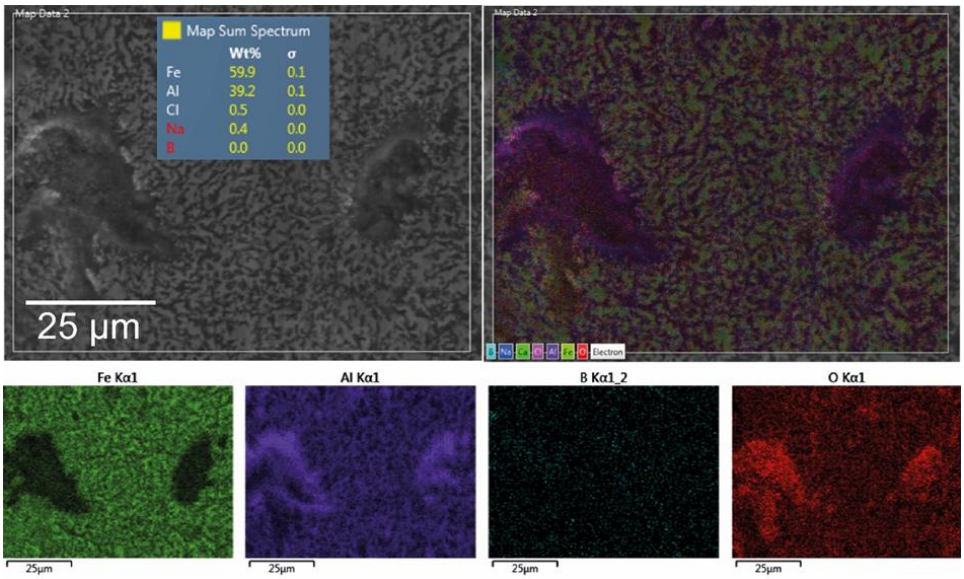

Figure 12. SEM and EDS images of boro-aluminized R4 steel after tribocorrosion test

4. CONCLUSION

This study investigates the characteristics of the boron-aluminide coating produced on R4 steel and its effectiveness in enhancing the corrosion resistance of the substrate. Following main results can be concluded from this study. The final coating comprised of three zones: a B-rich zone, FeAl layer, and a substrate matrix. XRD analysis revealed the dominant phase of the coating to be FeAl, with minor amounts of FeB, Fe_2B, and Fe5Al8 phases present. The electrochemical tests indicated that the boron-aluminide coating improved the corrosion resistance of R4 steel in a 3.5% NaCl solution, leading to lower corrosion rates and better corrosion resistance than untreated R4 steel. The coating's ceramic structure and chemical stability acted as a barrier between the coating and the substrate, contributing to enhanced corrosion resistance. These results suggest that boron-aluminide coatings have the potential of application in marine environments characterized by simultaneous wear and corrosion. Additionally, the FeAl and Fe_2Al_5 phases in the coating may have potential

applications in high-temperature environments. Overall, this study provides insights into the development of advanced coatings for improving the corrosion resistance of steel substrates.

5. ACKNOWLEDGEMENTS

The author would like to thank Bartın University and Prof. Dr. Mustafa Sabri Gök for the usage of laboratory infrastructure.

6. CONFLICT OF INTEREST

Author(s) approve that to the best of their knowledge, there is not any conflict of interest or common interest with an institution/organization or a person that may affect the review process of the paper.

7. AUTHOR CONTRIBUTION

The author has full responsibility for the paper in determining the concept of the research, data collection, data analysis and interpretation of the results, preparation of the manuscript, and critical analysis of the intellectual content with the final approval.

8. REFERENCES

Alkan S., Comparative Hydrodynamic Analysis of Catenary and Tension Leg Moored Floating Offshore Wind Turbine. 1st International Conference on Energy Systems Engineering, November, 291–298, 2017.

Alkan S., Enhancement of Marine Corrosion and Tribocorrosion Resistance of Offshore Mooring Chain Steel By Aluminizing Process. Brodogradnja, 73(4), 131–159, 2022(a).

Alkan S., Evaluation of pitting susceptibility and tribocorrosion behaviors of AISI 304 stainless steel in marine environments. Proceedings of the Institution of Mechanical Engineers, Part J: Journal of Engineering Tribology, 237(4), 808-823, 2022(b).

Alkan S., Gök M. S. (2021). Effect of sliding wear and electrochemical potential on tribocorrosion behaviour of AISI 316 stainless steel in seawater. Engineering Science and Technology, an International Journal, 24(2), 524–532.

Alkan S., Gök M. S., Influence of plasma nitriding pre-treatment on the corrosion and tribocorrosion behaviours of PVD CrN, TiN and AlTiN coated AISI 4140 steel in seawater. Lubrication Science, 34(2), 67–83, 2022.

Angulo Á., Tang J., Khadimallah A., Soua S., Mares C., Gan T. H., Acoustic emission monitoring of fatigue crack growth in mooring chains. Applied Sciences (Switzerland), 9(11), 2019.

Du J., Wang H., Wang S., Song X., Wang J., Chang A., Fatigue damage assessment of mooring lines under the effect of wave climate change and marine corrosion. Ocean Engineering, 206(April), 2020.

Erdogan A., Boriding Temperature Effect on Micro-Abrasion Wear Resistance of Borided Tool Steel. Journal of Tribology, 141(12), 2019.

Erdogan A., Yener T., Doleker K. M., Korkmaz M. E., Gök M. S., Low-temperature aluminizing influence on degradation of nimonic 80A surface: Microstructure, wear and high temperature oxidation behaviors. Surfaces and Interfaces, 25, 101240, 2021.

Günen A., Micro-abrasion wear behavior of thermal-spray-coated steel tooth drill bits. Acta Physica Polonica A, 130(1), 217–222, 2016.

Günen A., Kanca Y., Karahan İ. H., Karakaş M. S., Gök M. S., Kanca E., Çürük A., A Comparative Study on the Effects of Different Thermochemical Coating Techniques on Corrosion Resistance of STKM-13A Steel. Metallurgical and Materials Transactions A: Physical Metallurgy and Materials Science, 49(11), 5833–5847, 2018.

Günen A., Keddam M., Alkan S., Erdoğan A., Çetin M., Microstructural characterization, boriding kinetics and tribo-wear behavior of borided Fe-based A286 superalloy. Materials Characterization, 186(February), 2022.

Hu T. L., Huang H. L., Gan D., Lee T. Y., The microstructure of aluminized type 310 stainless steel. Surface and Coatings Technology, 201(6), 3502–3509, 2006.

IACS., Unified IACS Requirements Concerning Materials and Welding – W22 Offshore Mooring Chain. DNV-OS-E30(1993), 28, 2013.

Jiajia W. U., Tan F., Zhang D., Yin J., Li E., Corrosion of Copper-bearing High Strength Mooring Chain Steel Affected by Microbes in Seawater. Protection of Metals and Physical Chemistry of Surfaces, 55(6), 1207–1216, 2019.

Li W., Chen H., Li C., Huang W., Chen J., Zuo L., Ren Y., He J., Zhang S., Microstructure and tensile properties of AISI 321 stainless steel with aluminizing and annealing treatment. Materials and Design, 205, 109729, 2021.

López-Ortega A., Arana J. L., Rodríguez E., Bayón R., Corrosion, wear and tribocorrosion performance of a thermally sprayed aluminum coating modified by plasma electrolytic oxidation technique for offshore submerged components protection. Corrosion Science, 143(July), 258–280, 2018.

López-Ortega A., Areitioaurtena O., Alves S. A., Goitandia A. M., Elexpe I., Arana J. L., Bayón R., Development of a superhydrophobic and bactericide organic topcoat to be applied on thermally sprayed aluminum coatings in offshore submerged components. Progress in Organic Coatings, 137(September), 2019.

López-Ortega A., Bayón R., Arana J. L., Evaluation of protective coatings for offshore applications. Corrosion and tribocorrosion behavior in synthetic seawater. Surface and Coatings Technology, 349(May), 1083–1097, 2018.

López-Ortega A., Bayón R., Arana J. L., Arredondo A., Igartua A., Influence of temperature on the corrosion and tribocorrosion behaviour of High-Strength Low-Alloy steels used in offshore applications. Tribology International, 121(November 2017), 341–352, 2018.

López-Ortega A., Bayón R., Arana J. L., Evaluation of protective coatings for high-corrosivity category atmospheres in offshore applications. Materials, 12(8), 2019.

Ma K., Shu H., Smedley P., L'Hostis D., Duggal A., A Historical Review on Integrity Issues of Permanent Mooring Systems. One Petro. Offshore Technology Conference, May, 2013.

Marques F., Da Silva W. M., Pardal J. M., Tavares S. S. M., Scandian C., Influence of heat treatments on the micro-abrasion wear resistance of a superduplex stainless steel. Wear, 271(9–10), 1288–1294, 2011.

Moghaddam B. T., Hamedany A. M., Taylor J., Mehmanparast A., Brennan F., Davies C. M., Nikbin, K., Structural integrity assessment of floating offshore wind turbine support structures. Ocean Engineering, 208(May), 107487, 2020.

Ouladsaad S., Allaoui O., Daas A., Boro-aluminizing of XC38 steel. Indian Journal of Chemical Technology, 26(3), 239–243, 2019.

Öksüzoğlu E., Döleker K. M., 904L Paslanmaz Çeliğe Düşük Sıcaklık Alüminyumlamanın Etkisi. European Journal of Science and Technology, 28, 1102–1106, 2021.

Pandim T., Doca T., Figueiredo A. R., Pires F. M. A., Torsional fretting wear experimental analysis of a R3 offshore steel against a PC/ABS blend. Tribology International, 143(July 2019), 2020.

Pardo A., Merino M. C., Coy A. E., Viejo F., Arrabal R., Matykina, E., Pitting corrosion behaviour of austenitic stainless steels - combining effects of Mn and Mo additions. Corrosion Science, 50(6), 1796–1806, 2008.

Shen H.P., Cheng X.Y., Li H., Zhang S.Y., Effect of Copper Alloy Element on Corrosion Properties of High Strength Mooring Chain Steel. HSLA Steels 2015, Microalloying 2015 and Offshore Engineering Steels 2015, 1201–1209, 2016.

Shen Y., Sahoo P. K., Pan Y., A study of composite coatings on 22mncrnimo steel for mooring chain. Surface Review and Letters, 25(3), 2018.

Yener T., Doleker K. M., Erdogan A., High temperature oxidation behavior of low temperature aluminized Mirrax® ESR steel. Materials Research Express, 6(11), 2019.

Zhang X., Hoogeland M., Influence of deformation on corrosion of mooring chain steel in seawater. Materials and Corrosion, 70(6), 962–972, 2019.

Zhang Y., Yin X., Yan F., Effect of halide concentration on tribocorrosion behaviour of 304SS in artificial seawater. Corrosion Science, 99, 272–280, 2015.